Harvesting Waste Thermal Energy Using a Carbon-Nanotube-Based Thermo-Electrochemical Cell

Renchong Hu,[†] Baratunde A. Cola,[§] Nanda Haram,[||] Joseph N. Barisci,[†] Sergey Lee,[†,¶] Stephanie Stoughton,[†] Gordon Wallace,[⊥] Chee Too,[⊥] Michael Thomas,[⊥] Adrian Gestos,[⊥] Marilou E. dela Cruz,[‡] John P. Ferraris,[†,‡] Anvar A. Zakhidov,[†] and Ray H. Baughman*,[†,‡]

[†]Alan G. MacDiarmid NanoTech Institute, [‡]Department of Chemistry, University of Texas at Dallas, Richardson, Texas 75083, [§]George W. Woodruff School of Mechanical Engineering, Georgia Institute of Technology, Atlanta, Georgia 30332, [||]Department of Engineering Sciences, Maharashtra Academy of Engineering, Alandi (D), Pune 412 105, India, and [⊥]Intelligent Polymer Research Institute ARC Centre of Excellence for Electromaterials Science, University of Wollongong, Northfields Avenue, Wollongong, NSW 2522, Australia

ABSTRACT Low efficiencies and costly electrode materials have limited harvesting of thermal energy as electrical energy using thermo-electrochemical cells (or "thermocells"). We demonstrate thermocells, in practical configurations (from coin cells to cells that can be wrapped around exhaust pipes), that harvest low-grade thermal energy using relatively inexpensive carbon multiwalled nanotube (MWNT) electrodes. These electrodes provide high electrochemically accessible surface areas and fast redox-mediated electron transfer, which significantly enhances thermocell current generation capacity and overall efficiency. Thermocell efficiency is further improved by directly synthesizing MWNTs as vertical forests that reduce electrical and thermal resistance at electrode/substrate junctions. The efficiency of thermocells with MWNT electrodes is shown to be as high as 1.4% of Carnot efficiency, which is 3-fold higher than for previously demonstrated thermocells. With the cost of MWNTs decreasing, MWNT-based thermocells may become commercially viable for harvesting low-grade thermal energy.

KEYWORDS Thermo-electrochemical cells, thermogalvanic cells, thermocells, carbon nanotubes, thermal energy harvesting, low-grade waste heat

Low-grade heat (temperature below 130 °C), from such sources as industrial waste streams, geothermal activity, and solar heating, is projected to be a major sustainable energy source.[1,2] For many years the research community has focused on using solid-state thermoelectrics and Stirling engines to efficiently harvest low-grade heat as electrical energy. However, despite much progress over the past decades, current thermoelectric energy conversion technology is not very cost-effective and is constrained by physical and material limitations,[3] and Stirling engine technology is disadvantaged by high initial cost and problems with long-term reliability.[4] Thermo-electrochemical cells (otherwise known as thermogalvanic cells or thermocells) that utilize the temperature dependence of electrochemical redox potentials (i.e., the Seebeck effect) to produce electrical power may become an attractive alternative for harvesting low-grade heat, given their simple design, direct thermal-to-electric energy conversion, continuous operation, low expected maintenance, and zero carbon emission.[5-7]

The electrochemical Seebeck effect was first demonstrated over 100 years ago.[8,9] For a hypothetical redox system B ⇌ ne⁻ + A, the Seebeck coefficient, S, can be expressed as

$$S = \frac{\partial V}{\partial T} = \frac{\Delta S_{B,A}}{nF} \qquad (1)$$

where V is the electrode potential, T is temperature, n is the number of electrons involved in the reaction, F is Faraday's constant, and $\Delta S_{B,A}$ is the reaction entropy for the redox couple.[10,11] Thermocells using aqueous potassium ferrocyanide/ferricyanide redox solution have been studied by many groups because this redox system reversibly exchanges one electron per iron atom and produces a large reaction entropy, yielding Seebeck coefficient (>1 mV/K) and high exchange current.[11-16] However, to obtain efficiencies of reasonable interest noble metals such as Pt are usually required as electrode materials in thermocells, and this restricts commercial viability.[14-18] Also, the best prior-art thermocells typically have efficiencies of ~0.40% of Carnot efficiency (when efficiency is correctly evaluated, as discussed below).[15,16] In fact, it was previously predicted that a power conversion efficiency of 1.2% of the Carnot efficiency would be difficult to achieve.[15]
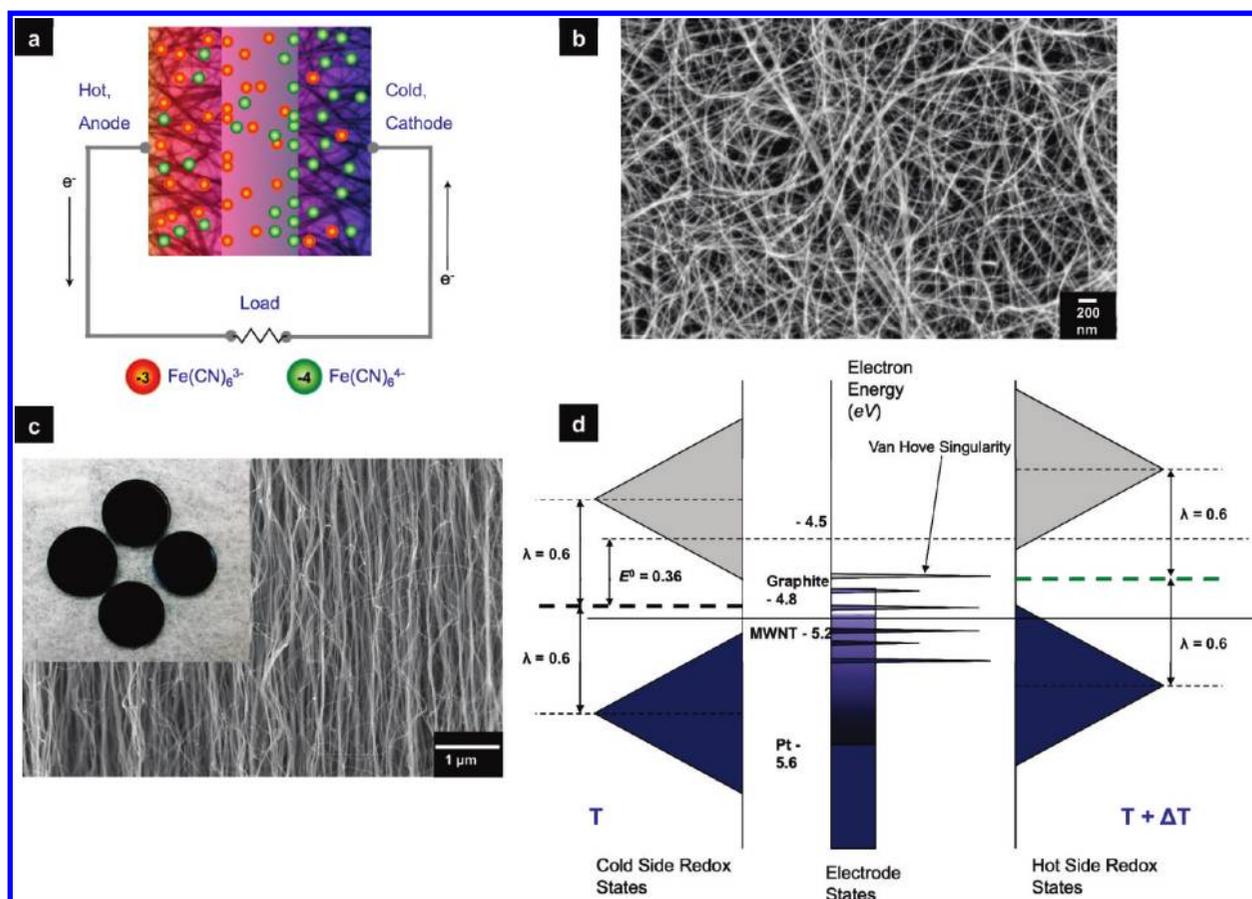
FIGURE 1. (a) Schematic of a thermocell with nanostructured electrodes showing concentration gradients of the ferri—ferrocyanide redox ions during power generation. (b) SEM micrograph of MWNT buckypaper. The average MWNT diameter is 10 nm. (c) SEM micrograph of vertical MWNT forest. The average MWNT diameter is approximately 20 nm. The inset shows coinlike stainless steel substrates fully coated with vertical MWNTs. Each substrate has a diameter of 2 cm. (d) Gerischer—Marcus model for the thermocell. The Van Hove singularities for MWNTs are shown close to the Fermi level. E^0 is the standard potential of $Fe(CN)_6^{3-}/Fe(CN)_6^{4-}$, λ is the reorganization energy of $Fe(CN)_6^{3-}/Fe(CN)_6^{4-}$ redox reactions.[46]

Carbon nanotubes (CNTs) have been of considerable interest for electrochemical applications, due to their exceptional electronic, mechanical, and chemical properties.[19-24] Advanced electrodes that incorporate CNTs have been shown to provide attractive performance for electrochemical applications (e.g., batteries, supercapacitors, and fuel cells[25-32]), due to their high surface area, ability to carry large current densities, and fast electron transfer kinetics.[33-35]

We here describe CNT-based thermocells that utilize the ferri/ferrocyanide redox couple and electrodes made from carbon-multiwalled nanotubes (MWNT) buckypaper and vertically aligned MWNT arrays (see Figure 1). This buckypaper is made by a filtration process that is analogous to that used for making ordinary paper. The performance of MWNTs as thermocell electrodes supersedes that of conventional electrode materials, including Pt foil and graphite sheet. With a hot-side temperature of 65 °C and a temperature difference of 60 °C, a maximum output power of 1.8 W/m² was achieved in a stagnant cell, corresponding to an efficiency relative to the Carnot cycle efficiency of 1.4%. Different designs were developed to demonstrate energy harvesting

in several practical scenarios. Our experiments revealed that the performance of MWNT-based thermocells is scalable, and that reduced contact resistance at MWNT electrode/substrate junctions can significantly enhance efficiency.

The power conversion efficiency of a thermocell is expressed as

$$\eta = \frac{1/4 V_{OC} I_{SC}}{Ak(\Delta T/d)} \quad (2)$$

and the relative power conversion efficiency is $\eta_r = \eta/(\Delta T/ T_h)$, where V_{OC} is the open circuit voltage, I_{SC} is the short circuit current, A is the cross-sectional area of the cell, d is the electrode separation distance, ΔT is the temperature difference between the two electrodes, k is the thermal conductivity of the electrolyte (or the effective thermal conductivity of the electrolyte and separator), and T_h is the temperature at the hot side. The maximum output power, P_{MAX}, is $1/4 V_{OC} I_{SC}$ and $Ak(\Delta T/d)$ is the input thermal energy needed to maintain ΔT. $\Delta T/T_h$ is the Carnot efficiency. As

previously described, erroneous assumptions have been often made in evaluating energy conversion efficiencies.[15] Efficiencies are also overestimated if the A in eq 1 is taken as the cross-sectional area of an electrode, and the effective area for ionic conduction and heat flow is much larger due to a larger cross-sectional area of the cell.

The efficiency of the thermocell can be more fundamentally expressed by combining eq 1 and eq 2 to give

$$\eta = \frac{1/4\Delta S_{B,A} j_{SC} R_T}{nF} \tag{3}$$

where j_{SC} ($=I_{SC}/A$) is the short circuit current density and R_T ($=d/k$) is the thermal resistance of the cell. The ferri/ferrocyanide redox couple, where $n = 1$, is known to produce a relatively high reaction entropy,[36] so we here focus on increasing the parameters that critically limit thermocell efficiency, j_{SC} and R_T. The intrinsically large surface area of MWNTs and fast electron transfer between MWNT electrodes and electrolyte directly enhance j_{SC}.[37−40] Thermal conduction losses are mitigated (i.e., R_T is increased) using two primary approaches that also enhance j_{SC}, (1) we took advantage of the highly porous three-dimensional structure of MWNT buckypaper by using scroll-like electrodes, which are commonly used in batteries and capacitors, to reduce cross-sectional area normal to the direction of heat flow while allowing a high degree of electrolyte exposure to the electrode surface for redox reactions to occur, and (2) we directly synthesized vertically aligned MWNT arrays (i.e., nanotube forests) to establish electrodes that are in good thermal and electrical contact with the thermocell packaging.[41,42]

The MWNT buckypaper was prepared according to procedures described in previous work.[43,44] The MWNTs are of high purity (containing less than 1% catalyst) and hundreds of micrometers long, with diameters of ∼10 nm. The MWNT buckypaper is typically ∼35 μm thick and has an electrical conductivity of 100 S/cm[44] and an internal surface area of 278 m²/g by the Brunauer−Emmett−Teller method. Figure 1b shows a scanning electron micrograph (SEM) of the MWNT buckypaper. Cyclic voltammograms (CV) show quasi-reversible electron transfer reactions between MWNT buckypaper electrodes and $Fe(CN)_6^{3-/4-}$ in aqueous electrolyte. The MWNT buckypaper also shows three times higher charging current density during CV scans than the same physical area Pt foil.

The electrical energy output of thermal electrochemical cells can be optimized by ensuring that the temperature drop is predominantly between the electrodes, rather than between the heat source and heat sink and the corresponding proximate electrodes. To reduce temperature drop from thermal contact resistance for thermal cells based on conventional coin cell battery containers, MWNT forests were directly synthesized on the internal stainless steel electrode surfaces of these coin cells. The MWNT forests were grown using a trilayer catalyst (30 nm Ti, 10 nm Al, and 2 nm Fe), plasma-enhanced CVD, and previously reported process conditions.[41] The MWNT forests were approximately 100 μm tall. Vertical alignment of MWNTs and good coverage of MWNTs on the surfaces of the packaging substrates is illustrated in Figure 1c. The thermal resistance at MWNT forest/substrate junctions was measured in previous work to be less than 0.01 cm²K/W, and the resistance of a solder joint, the buckypaper electrodes are effectively soldered to the packaging substrates in the coin cell configuration, is 5-fold higher than this value.[41] The electrolyte used for all thermocells in this work was 0.4 M $K_3Fe(CN)_6/K_4Fe(CN)_6$ aqueous solution, as this was demonstrated to be the optimum redox couple concentration.

The performance of MWNT buckypaper, Pt foil (Sigma-Aldrich Co.), and graphite sheet (98% graphite, GrafTech, Inc.) electrodes were directly compared using a U-shaped electrochemical cell. The hot side temperature was a constant 65 °C while the cold side temperature was 5 °C, the two electrodes were 5.0 cm apart, and each electrode sheet was 1.0 cm × 0.5 cm. Conductive Ag paste was used to promote good electrical contact between buckypaper electrodes and Pt wire leads. The contacts were then covered by insulating paint to prevent possible artifacts due to interaction between the Ag paste and the electrolyte. Every data point of V_{OC} and I_{SC} was acquired after allowing sufficient time for the values to stabilize. Similar Seebeck coefficients of 1.4 mV/K were measured for all the electrode materials, which is expected because the Seebeck coefficient is governed by the thermodynamics of the redox couple, not the electrode material, as shown in eq 1.

The j_{SC} and power (P_{MAX}) generated by the MWNT buckypaper electrodes for an optimized electrical load were the highest among the tested electrode materials, 64.6 A/m² and 1.36 W/m², respectively. The normalized current density, $j_{SC}/\Delta T$, was 1.08 A/(m²K) and the normalized area power density, $P_{MAX}/\Delta T^2$, was 3.8 × 10⁻⁴ W/(m²K²). The Pt electrodes generated a j_{SC} of 48.4 A/m² and a P_{MAX} of 1.02 W/m², corresponding to a $j_{SC}/\Delta T$ of 0.81 A/(m²K) and a $P_{MAX}/\Delta T^2$ of 2.8 × 10⁻⁴ W/(m²K²). The graphite sheet electrodes generated a j_{SC} of 36.6 A/m² and a P_{MAX} of 0.76 W/m², corresponding to a $j_{SC}/\Delta T$ of 0.61 A/(m²K) and a $P_{MAX}/\Delta T^2$ of 2.1 × 10⁻⁴ W/(m²K²). The MWNT buckypaper electrodes thus produced 33 and 77% higher $j_{SC}/\Delta T$ than Pt and graphite sheet electrodes, respectively. Previous work reported $j_{SC}/\Delta T = 0.5$ A/(m²K) and $P_{MAX}/\Delta T^2 = 2.0 \times 10^{-4}$ W/(m²K²) using Pt electrodes with the same interelectrode distance and only one side of each electrode exposed to electrolyte.[16] When we blocked one side of the anode and cathode with Scotch tape, $j_{SC}/\Delta T$ decreased 26% for the MWNT electrodes and decreased 28% for the Pt electrodes, which brings the present $j_{SC}/\Delta T$ for Pt electrodes into close agreement with this previous work.
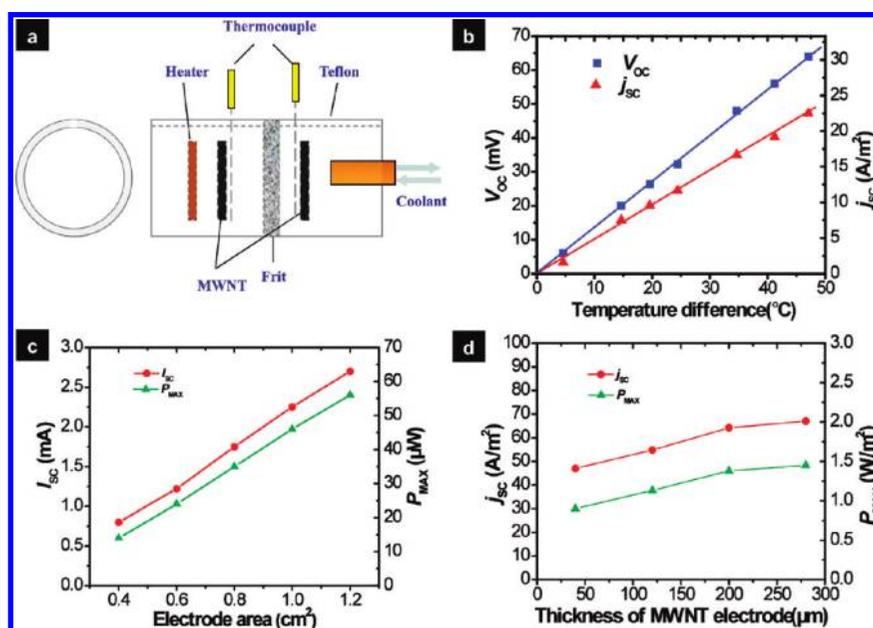
FIGURE 2. (a) The Teflon cell with adjustable interelectrode distance. The cell consists of a HOTWATT heater, a Cu rod sealed in Teflon tape with cold liquid circulating inside, a glass frit separator, and two OMEGA K-type thermocouples wrapped with Teflon tape. (b) V_{OC} and j_{SC} versus temperature difference between electrodes. The distance between electrodes, d, was 2.6 cm. Each electrode was 1.8 mg and 1.5 cm × 0.8 cm × 30 μm. (c) I_{SC} and P_{MAX} versus MWNT electrode area with $\Delta T = 47$ °C, $d = 2.6$ cm, MWNT buckypaper thickness 30 μm. (d) j_{SC} and P_{MAX} versus buckypaper electrode thickness with the area of each electrode fixed at 1.0 cm × 0.5 cm, $\Delta T = 60$ °C, $d = 2.6$ cm.

Upon reaching equilibrium, j_{SC} in the Nernst—Plank equation consists of diffusion current density $j_d = F\Sigma(z_n D_n \partial C_n/\partial x)$ and migration current density $j_m = F^2/RT(\partial V/\partial x)\Sigma(z_n^2 D_n C_n)$, where z_n is the charge, D_n is the diffusion coefficient, C_n is the ion concentration, R is the gas constant, and x is the distance from one electrode to the point of interest between the two electrodes (the other parameters are the same as defined above). Here j_m is similar in all cases because the potential differences across the electrodes are similar given the same ΔT. Therefore, j_d, or more specifically the concentration gradient, $\partial C_n/\partial x$, must be different for the Pt, MWNT, and graphite electrodes studied here. One reason for the relatively large j_{SC} (or j_d) generated by MWNT electrodes is the large number of redox reaction sites established by the high internal surface area of such electrodes. This surface area (or concentration gradient) advantage is likely the cause of MWNT electrodes producing higher current densities than Pt foil electrodes because the kinetics of the two materials appears to be similar within the resolution of our experiments (see Figure S1 of Supporting Information). However, high-surface-area activated carbon fabric (Spectracarb 2225 from Engineered Fibers Technology, LLC with an internal surface area of 2500 m²/g) yielded a low $j_{SC}/\Delta T$ of 0.05 A/(m²K) (evaluated using geometric area) when tested in the U-shaped cell, which implies that surface area enhancements alone are not sufficient to generate large j_{SC}. The comparisons of the cyclic voltammetry (CV) scans for MWNT and graphite sheets in Figure S1 of Supporting Information clearly indicate slower electron transfer on graphite electrodes. It has been suggested that electron transfer at the MWNT/electrolyte interface is enhanced as a result of fast kinetics.[39] The improved kinetics over other carbon materials such as graphite sheet is likely the result of the quasi-one-dimensional crystalline structure of MWNTs and their resulting highly localized electron density of states near the Fermi level (i.e., Van Hove singularities).[45] The Gerischer—Marcus model in Figure 1d illustrates this kinetic effect.

The Teflon cell shown in Figure 2a was used to evaluate performance scaling with ΔT. The distance between two equivalent size MWNT buckypaper electrodes was set at 2.6 cm. The hot side was maintained at 70 °C using a resistive heater connected to a temperature controller and the cold side temperature was adjusted by circulating coolant from a thermostat bath. As shown in Figure 2b, both V_{OC} and j_{SC} increase linearly with ΔT, indicating the cell operates within a linear region. Variation of external load resistance resulted in linear variation of cell current on the voltage drop across the load resistor, so output power was optimized when effective internal cell resistance equaled the external load resistance. The cell in Figure 2a was also used to test the feasibility of making larger MWNT-based thermocell devices (these tests were conducted with ΔT fixed). As shown in Figure 2c, increasing the electrode area from 0.4 to 1.2 cm² increased the short circuit current from 0.8 to 2.7 mA and increased the maximum power output from 16 to 55 μW. For the given range of electrode sizes, a linear relationship between thermocell performance and electrode area is clearly shown, indicating scalability toward larger devices. When the thickness of buckypaper electrodes with fixed area was increased from 40 to 280 μm, j_{SC} increased from 47 to
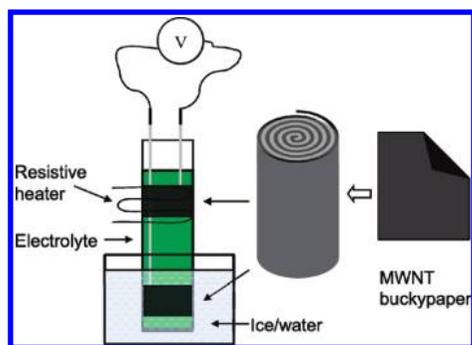
FIGURE 3. Mark II cell with MWNT scrolls as electrodes. Two thermocouples (not shown) were used to measure temperature in the cell near the hot and cold electrodes.

67 A/m^2 and P_{MAX} increased from 0.9 to 1.45 W/m^2 (see Figure 2d). The dependencies of j_{SC} and P_{MAX} on buckypaper sheet thickness were nonlinear and a saturation thickness was evident during testing, likely because diffusion of the redox mediator through increasing thickness sheets becomes a limiting factor. To demonstrate voltage and power scaling, two identical thermocells (as shown in Figure S4 of Supporting Information) were connected in series. The open circuit voltage for the combined cells was 140 mV, which is equal to the sum of the open circuit voltages of the individual cells. The maximum output power of the combined cells was 101.5 μW, which approximately equals the sum of the maximum output powers of the two cells when they are individually operated (see Table S2 of Supporting Information).

The electrode spacing is adjustable in the cell shown in Figure 2a. When electrode separation distance was decreased, both j_{SC} and P_{MAX} increased because ions could diffuse quickly over shorter distances, that is, ionic mass transport was enhanced; yet, efficiency dropped significantly because a higher thermal energy input was required to maintain the same ΔT. Similar observations were made in a previous study.[16] We here addressed this trade-off between current density and heat loss by forming MWNT buckypaper into scrolls and aligning them along the rolling axis to minimize the heat loss channel and increase j_{SC}. Two buckypaper scroll electrodes, each having a diameter of 0.3 cm and weighing 0.5 mg, were positioned in a glass tube with a diameter of 0.3 cm so that the scroll ends faced each other (this configuration is shown as Mark II in Figure 3). The distance between the electrodes was $d = 5.0$ cm. The hot side was held at 65 °C by a temperature controller and the cold side of the cell was immersed in a mixture of ice/water and had a temperature of 5 °C. A j_{SC} of 85 A/m^2, or $j_{SC}/\Delta T$ of 1.42 A/(m^{2}K), and a P_{MAX} of 1.8 W/m^2, or $P_{MAX}/\Delta T^2$ of 5 × 10^{-4} W/(m^{2}K^2), were measured based on the cross-section area of the cell. The power conversion efficiency for the Mark II thermocell is 0.24%, which is approximately an order of magnitude higher than values obtained in prior work using Pt electrodes under similar test conditions.[16] The relative efficiency is 1.4%, which is 17% higher than a previously estimated upper bound for thermocells using the ferri/ferrocyanide redox couple.[15]

Thin coin-type thermocells with MWNT buckypaper and vertically aligned forest electrodes, which could potentially be powered by body heat, were used to evaluate the feasibility of stable long-term performance and scalable device fabrication (see Figure 4a). The thermocells were constantly discharged through a resistor load of 10 Ω. For a nominal ΔT of 45 °C, voltage was 51.2 mV and current density stabilized at 30.4 A/m^2 in the coinlike thermocell with buckypaper electrodes (see Figure 4b). For a nominal ΔT of 60 °C, V_{OC} was 70.4 mV and j_{SC} stabilized at 55.7 A/m^2 ($j_{SC}/\Delta T = 0.93$ A/(m^{2}K)) in the coinlike thermocell with MWNT forest electrodes (see Figure 4c). Because of vertical nanotube alignment that ostensibly improves electrolyte access to MWNT surfaces, and because of improved thermal and electrical contact to the packaging substrates,[41,42] the efficiency of coinlike thermocells with MWNT forest electrodes was approximately 30% higher than the efficiency of coin cells with buckypaper electrodes (we estimate that approximately 4 °C of temperature was lost across the less intimate buckypaper/substrate junctions).

Concerns about the stability of potassium ferrocyanide/ferricyanide, especially upon illumination, have been reported.[47,48] Previous work also reported the possibility of mass transport overpotential leading to detrimental buildup of concentration gradient in the cell, in particular the establishment of higher electrolyte concentration at the cold side. Such claims suggest a decline in current if thermocells are subject to long-term discharge. However, as shown in Figure 4, the coinlike thermocell with buckypaper electrodes was successfully continuously discharged over a 10 Ω load for more than three months, and the coinlike thermocell with MWNT forest electrodes was continuously discharged for a week with no change in performance. For each test the circuits were disconnected only when measuring V_{OC}, which takes about 5 min per data point. Both voltage and the discharged current were stable during long-term testing, which demonstrates the stability of the aqueous equimolar redox solution in closed systems. We posit that this level of stability occurs because the electrolyte reaches equilibrium and the MWNTs are very stable in the solution within the temperature range. The demonstrated stability of MWNT-based thermocells during continuous use suggests that if the heat source is stable the power generation will always operate at near 100% capacity.

A thermocell produces its maximum V_{OC} once the difference in redox ion concentration at the electrodes reaches its highest value and the electron transfer process at the electrode/electrolyte interfaces reach equilibrium. It can take as much as 10 min for this to occur in a thermocell where the electrolyte is stagnant, as shown in Figure 5c. The actual equilibrium time depends on partially the amount of electrolyte around the electrode with more electrolyte requiring
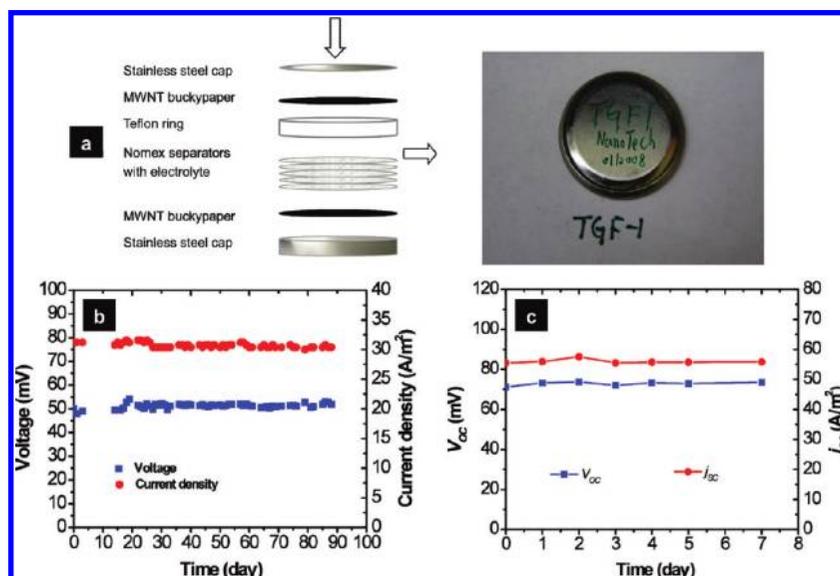
FIGURE 4. (a) Schematic assembly of the coinlike thermocell. Each buckypaper electrode is 0.5 cm $\times$ 0.5 cm and attached to the package with Ag paste. The MWNT forest electrodes are grown directly on the caps as shown in Figure 1c. The electrodes are separated by five layers of Nomex HT4848 soaked with electrolyte. The cells are sealed by pneumatic crimping. The cell diameter is 2.0 cm and height is 0.2 cm. (b) Voltage and current versus operation time for a coin cell with buckypaper electrodes discharging over a 10 Ω load. The nominal ΔT was 45 °C (variation <3%). (c) V_{OC} and j_{SC} versus time for coin cell with MWNT forest electrodes. The nominal ΔT was 60 °C.

longer time. After the maximum V_{OC} was reached, shorting the circuit for the "stagnant" thermocell in Figure 5c decreased j_{SC} from its peak value of 105 A/m^2 to approximately half its peak value, 49 A/m^2. To sustain j_{SC} at its maximum value consumed redox ions must be replenished fast enough at the electrode/electrolyte interfaces to eliminate the limiting effects of mass transport via sluggish ion diffusion. Stirring or circulating the electrolyte to quickly deliver fresh electrolyte to the electrodes can achieve this, and such approaches have been demonstrated to increase j_{SC} in thermocells with Pt electrodes.[37] A MWNT-based thermocell with circulated electrolyte (i.e., a "flow" cell) is shown in Figures 5a,b. A pump located between each compartment and an electrolyte reservoir associated with each compartment circulated the electrolyte. The temperatures of the hot and cold reservoirs were held constant by a temperature-controlled heater and heat sink, respectively. Each compartment contained one MWNT buckypaper electrode that was 1.2 cm $\times$ 0.5 cm. Stagnant and flow MWNT-based thermocells driven by the same ΔT are compared in Figure 5c. Notably, V_{OC} and j_{SC} were maintained in the flow thermocell at the stagnant cell peak values because fresh electrolyte was constantly delivered to the electrodes as discussed above. For the flow cell with MWNT electrodes, $j_{SC}/\Delta T$ reached 1.12 A/(m^{2}K), while the stagnant cell provided only 0.6 A/(m^{2}K). For comparison, the flow cell using Pt electrodes provided a $j_{SC}/\Delta T$ of 0.89 A/(m^{2}K), which is close to previously reported maximum value for a similar Pt electrode flow cell.[37] The $P_{MAX}/\Delta T^2$ of the MWNT electrode flow cell reached 4×10^{-4} W/(m^{2}K^2), as compared with 2×10^{-4} W/(m^{2}K^2) for the stagnant cell. As shown in Figure 5d, the flow thermocell produced stable V_{OC} and j_{SC} during 8 days of

testing, which suggests that stable performance can be achieved in long-term operation.

Because numerous pipes that carry hot or cold fluids are installed in facilities such as power and chemical processing plants, a thermocell wrapped around a pipe is demonstrated as a candidate technology for harvesting these rich supplies of energy. Such pipes can serve as hot or cold sources for thermocells with the ambient regulating the temperature of the electrode not in contact with the pipe (imagine steam flowing through a pipe located in Alaska as a potential scenario for this energy harvesting concept). Here we demonstrate a thin thermocell configuration wrapped around a stainless steel pipe with cool liquid flowing within (ammonia flowing through a pipe in a chemical plant in Florida is a candidate scenario). The pipe assembly consisted of a first layer of MWNT buckypaper electrode, then two layers of Nomex HT4848 as separator, and an outer layer of MWNT buckypaper electrode. A piece of stainless steel sheet was wrapped around the outer layer buckypaper and two clamps and glue were used to seal the entire assembly. A resistive heater was wrapped around the stainless steel sheet. Electrolyte was injected using a syringe, and afterward the syringe hole was sealed with glue. The schematic layout and actual assembly of the pipe-wrapped thermocell is shown in Figure 6. This cell produced a V_{OC} of 21 mV, which corresponds to a ΔT of 15 °C across the thin layer structure, and a j_{SC} and P_{MAX} of 7.5 A/m^2 ($j_{SC}/\Delta T = 0.5$ A/(m^{2}K)) and 0.039 W/m^2 ($P_{MAX}/\Delta T^2 = 1.8 \times 10^{-4}$ W/(m^{2}K^2)), respectively.

The cost of renewable energy technologies per unit watt of generated power is a metric that greatly affects commercial viability assuming similar product lifetimes. The material cost of coinlike thermocells includes the cost of the
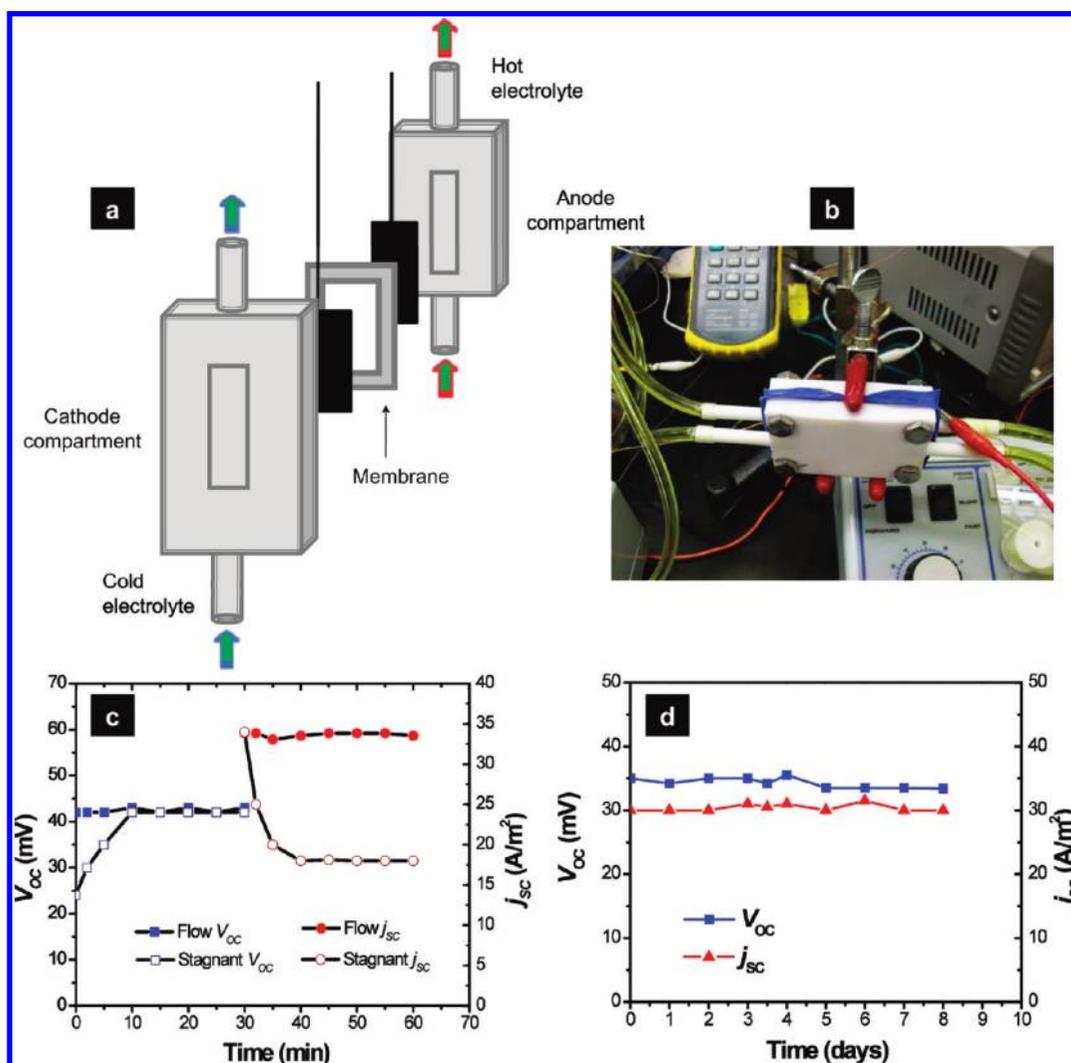
FIGURE 5. (a) Schematic assembly of the Teflon flow thermocell. The two compartments are separated by a cellular ester membrane (Whatman) and two layers of Nomex fabric. (b) Photograph of the flow thermocell setup. (c) Transitional V_{OC} and j_{SC} in a stagnant and flow cell. (d) Performance of flow cell with MWNT buckypaper electrodes versus time. Each electrode was 1.2×0.5 cm. The nominal ΔT approximately 50 °C.
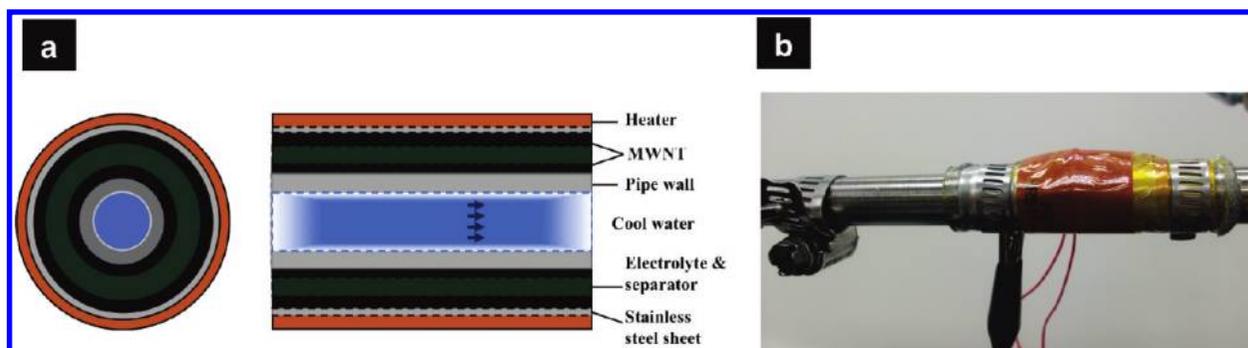
FIGURE 6. (a) Schematic assembly of the thin thermocell wrapped around a pipe carrying cool, flowing liquid. Two layers of Nomex are used to separate the two electrodes. The distance between electrodes is approximately 0.2 cm. (b) Photograph of a thermocell wrapped around a stainless steel pipe to generate power.

electrochemically active potassium ferri—ferrocyanide and MWNTs. The current cost per watt of active materials for

these cells operating at a ΔT of 60 °C is estimated to be \$5.14/W, which is slightly higher than the cost per watt of

photovoltaic modules.[49] If current predictions are realized and the price of MWNTs decreases to $45/kg from today's price of ~$150/kg, we estimate that the material cost of active materials for coinlike thermocells will reach $2.76/W. Since the output power of these thermocells increases quadratically with ΔT, development of electrolytes that can operate to higher temperatures can substantially increase applications potential. Though the present continuously operated thermal cells provided essentially constant output for the maximum evaluated time period (90 days), operational lifetimes of years or decades will be desirable for some applications and this might require improvements in the choice of electrolyte and redox mediator. Also, we are here assuming that the waste energy is essentially free and unlimited, since the relatively low conversion efficiencies of even the presently improved thermocells is a problem if cost-effective technologies having higher efficiencies become available.

In summary, we have shown that MWNT buckypaper and MWNT forest are efficient electrode materials for thermocells because they offer fast kinetics and large amounts of electrochemically accessible internal surface area. The efficiency of thermocells with MWNT electrodes was demonstrated to be as high as 1.4% relative to the Carnot Cycle, which is 3 times higher than the efficiency of conventional thermocell devices with Pt electrodes. With improvements in cell design and optimization of MWNT properties and electrode structure, thermocell efficiency is likely to increase. Thin coinlike thermocells were fabricated and operated for three months to provide essentially constant power output. In such configurations, direct synthesis of MWNT forest electrodes was shown to provide improved thermal contact that contributed to a 30% increase in efficiency as compared to buckypaper electrodes that required secondary attachment to the package substrates. The performance of MWNT-based thermocells was shown to be scalable and amenable to complex systems. With the cost of MWNTs decreasing, thermocells with the performance reported here may develop into an economical solution for harvesting untapped supplies of low-grade heat. Moreover, the enhanced thermocell performance demonstrated in this study using MWNT electrodes suggests that other nanostructured electrode materials might also be applied to significantly enhance the efficiency of thermocell devices.

Supporting Information Available. CV scans of Pt, graphite sheet, and MWNT buckypaper electrodes in $Fe(CN)_6^{3-/4-}$ aqueous electrolyte; U-shaped thermocell; Mark I thermocell configuration and performance; performance of Mark I thermocells in series; performance versus electrolyte concentration; effect of interelectrode distance; detailed cost analysis. This material is available free of charge via the Internet at http://pubs.acs.org.

REFERENCES AND NOTES

(1) Innovative Energy Systems Challenge; Funding Opportunity Number DE-PS36-06GO96009; U.S. Department of Energy: Washington, DC, 10/20/2005.
(2) *The Future of Geothermal Energy*; MIT-led interdisciplinary panel; Massachusetts Institute of Technology, 2006.
(3) Vining, C. B. *Nat. Mater.* **2009**, *8*, 83.
(4) Mancini, T.; Heller, P.; Butler, B. *J. Sol. Energy Eng.* **2003**, *125*, 135.
(5) Agar, J. N. In *Advances in Electrochemistry and Electrochemical Engineering*; Delahay, P., Tobias, C. W., Eds.; J. Wiley & Sons: New York, 1961; Vol. 3, Chapter 4.
(6) Haase, R. *Thermodynamics of Irreversible Processes*; Addison-Wesley: Reading, MA, 1962.
(7) Ratkje, S. K.; Ikeshoji, T. *J. Electrochem. Soc.* **1990**, *137*, 2088.
(8) Coggeshall, G. W. *Z. Phys. Chem.* **1895**, *24*, 62.
(9) Richards, T. W. *Z. Phys. Chem.* **1897**, *24*, 39.
(10) Eastman, E. D. *J. Am. Chem. Soc.* **1928**, *50*, 292.
(11) Quickenden, T. I.; Vernon, C. F. *Solar Energy* **1986**, *36*, 63.
(12) Ikeshoji, T. *Bull. Chem. Soc. Jpn.* **1987**, *60*, 1505.
(13) Ikeshoji, T. F.; Nahui, N. B.; S. Kimura, S.; Yoneya, M. *J. Electroanal. Chem.* **1991**, *312*, 43.
(14) Burrows, B. *J. Electrochem. Soc.* **1976**, *123*, 154.
(15) Quickenden, T. I.; Mua, Y. *J. Electrochem. Soc.* **1995**, *142*, 3985.
(16) Mua, Y.; Quickenden, T. I. *J. Electrochem. Soc.* **1996**, *143*, 2558.
(17) Shindo, K.; Arakawa, M.; Hirai, T. *J. Power Sources* **1998**, *70*, 228.
(18) deBethune, A. J.; Licht, T. S.; Swendeman, N. *J. Electrochem. Soc.* **1959**, *106*, 616.
(19) Wang, J. *Trends Anal. Chem.* **2002**, *21*, 226.
(20) Wang, J. *Acc. Chem. Res.* **2002**, *35*, 811.
(21) Britto, P. J.; Santhanam, K. S. V.; Rubio, A.; Alonso, J. A.; Ajayan, P. M. *Adv. Mater.* **1999**, *11*, 154.
(22) Gooding, J. J. *Electrochim. Acta* **2005**, *50*, 3049.
(23) Merkoci, A.; Pumera, M.; Llopis, X.; Perez, B.; del Valle, M.; Alegret, S. *Trends Anal. Chem.* **2005**, *24*, 826.
(24) Gong, K.; Yan, Y.; Zhang, M.; Su, L.; Xiong, S.; Mao, L. *Anal. Sci.* **2005**, *21*, 1383.
(25) Rajesh, B.; Thampi, K. R.; Bonard, J. M.; Xanthopoulos, N.; Mathieu, H. J.; Viswanathan, B. *J. Phys. Chem. B* **2003**, *107*, 2701.
(26) Li, W. Z.; Liang, C. H.; Zhou, W. J.; Qiu, J. S.; Li, H. Q.; Sun, G. Q.; Xin, Q. *Carbon* **2004**, *42*, 436.
(27) Matsumoto, T.; Komatsu, T.; Nakano, H.; Arai, K.; Nagashima, Y.; Yoo, E.; Yamazaki, T.; Kijima, M.; Shimizu, H.; Takasawa, Y.; Nakamura, J. *Catal. Today* **2004**, *90*, 277.
(28) He, Z. B.; Chen, J. H.; Liu, D. Y.; Tang, H.; Deng, W.; Kuang, W. F. *Mater. Chem. Phys.* **2004**, *85*, 396.
(29) Che, G.; Lakshmi, B. B.; Fisher, E. R.; Martin, C. R. *Nature* **1998**, *393*, 346.
(30) Frackowiak, E.; Beguin, F. *Carbon* **2001**, *39*, 937.
(31) Niu, C.; Sichel, E. K.; Hoch, R.; Roy, D.; Tennent, H. *Appl. Phys. Lett.* **1997**, *70*, 1480.
(32) Baughman, R. H.; Zakhidov, A. A.; de Heer, W. A. *Science* **2002**, *297*, 787.
(33) Campbell, J. K.; Sun, L.; Crooks, R. M. *J. Am. Chem. Soc.* **1999**, *121*, 3779.
(34) Cai, H.; Cao, X.; Jiang, Y.; He, P.; Fang, Y. *Anal. Bioanal. Chem.* **2003**, *375*, 287.
(35) Zhang, N.; Xie, J.; Varadan, V. K. *Smart Mater. Struct.* **2006**, *15*, 123.
(36) Hupp, J. T.; Weaver, M. J. *Inorg. Chem.* **1984**, *23*, 3639.
(37) Josserand, J.; Devaud, V.; Lagger, G.; Jensen, H.; Girault, H. H. *J. Electroanal. Chem.* **2004**, *565*, 65.

(38) Baughman, R. H.; Cui, C.; Zakhidov, A. A.; Iqbal, Z.; Barisci, J. N.; Spinks, G. M.; Wallace, G. G.; Mazzoldi, A.; De Rossi, D.; Rinzler, A. G.; Jaschinski, O.; Roth, S.; Kertesz, M. *Science* **1999**, *284*, 1340.

(39) Nugent, J. M.; Santhanam, K. S. V.; Rubio, A.; Ajayan, P. M. *Nano Lett.* **2001**, *1*, 87.

(40) Andrews, R.; Jacques, D.; Qian, D.; Rantell, T. *Acc. Chem. Res.* **2002**, *35*, 1008.

(41) Cola, B. A.; Xu, J.; Cheng, C.; Xu, X.; Hu, H.; Fisher, T. S. *J. Appl. Phys.* **2007**, *101*, No. 054313.

(42) Park, M.; Cola, B. A.; Siegmund, T.; Xu, J.; Maschmann, M. R.; Fisher, T. S.; Kim, H. *Nanotechnology* **2006**, *17*, 2294.

(43) Zhang, M.; Atkinson, K. R.; Baughman, R. H. *Science* **2004**, *306*, 1358.

(44) Hall, L. J.; Coluci, V. R.; Galvão, D. S.; Kozlov, M. E.; Zhang, M.; Dantas, S. O.; Baughman, R. H. *Science* **2008**, *320*, 504.

(45) Schonenberger, C.; Bachtold, A.; Strunk, C.; Salvetat, J.-P.; Forro, L. *Appl. Phys. A: Mater. Sci. Process.* **1999**, *69*, 283.

(46) Morisaki, H.; Ono, H.; Yazawa, K. *J. Electrochem. Soc.* **1989**, *136*, 1710.

(47) MacDiarmid, A. G.; Hall, N. F. *J. Am. Chem. Soc.* **1953**, *75*, 5204.

(48) MacDiarmid, A. G.; Hall, N. F. *J. Am. Chem. Soc.* **1954**, *76*, 4222.

(49) As of Dec. 29, 2009, the solar module price in the United States market is $4.31 per Watt of peak power according to http://solarbuzz.com/moduleprices.htm.